Use of Au nanoparticles in radiotherapy and diagnostics

N. Restuccia [1] and L. Torrisi[1]

[1] *Dipartimento di Scienze Matematiche e Informatiche, Scienze Fisiche e Scienze della Terra, viale F. Stagno d'Alcontres 31, Messina, Italy*

E-mail: nrestuccia@unime.it

Abstract

Radiation therapy and diagnostics, usually done with x-rays or electrons beams, may be improve increasing the equivalent atomic number of the target. The use of Au nanoparticles placed in tumor tissues allows of significantly increase of the deposited dose compared to healthy tissue. Au nanoparticles were prepared by laser ablation in water to be injected locally in tumor sites. Using the NIST database for x-ray absorption coefficients and stopping powers of electrons and protons in tissues (water equivalent, adipose tissue and cortical bone) with and without the injection of Au nanoparticles it was possible to evaluate the dose increment not only traditional and innovative radiotherapy using hadrons beams receive benefit, because medical diagnostics can taken advantage for imagining, due to the images contrast increase.

Keywords: Nanoparticles, Radiotherapy, Diagnostics.

Introduction

In recent years, the technological development has permitted to manipulate and to characterize nanosized materials and systems. Metal nanoparticles (NP) have numerous applications: electronics (detectors, solar cells, optoelectronics), telecommunications (nonlinear optics, nanophotonics, nanotermica), biology and medicine (photothermal therapy, radiation and biological imaging marking) and physical chemistry (catalysts, targets preparation)[1]. Metals nanoparticles embedded in an insulating medium have a behavior similar to absorbent centers of ionizing radiation, they show a resonant absorption band at specific wavelengths depend on used elements. Their uniform distribution changes the electron density and the equivalent atomic number of medium. Thanks to the submicrometrics dimensions functionalized Au nanoparticles can be easily internalized in byological systems, like organs and single cells, and make they absorbent at ionizing radiation (X-ray, electrons and ions) and non-ionizing radiation(IR, laser beams and visible light). The choice of gold as a starting material is not accidental, it is known that the gold in bulk form is biocompatible for humans and, more in general, also for other living beings. The medicine shows a particular interest to the Au nanoparticles. Infact also durgs fuctionalized Au are use in pharmacoloy for treatment of rheumatoid arthritis. In the present study it was determined experimentally the behavior of Au nanoparticles in therapy and in diagnostics, in particular by calculating the ratio of the dose delivered to a given depth and the dose delivered to the surface in various media (water equivalent, adipose tissues and bone compact). The anti-cancer potential of the Au nanoparticles is due to by many advantageous physico-chemical properties. Many studies have demonstrated the safety and biocompatibility of gold in vitro and in vivo, suggesting that the gold nanoparticles can be administered safely with minimal inflammatory activation and few local or systemic side effects [2].

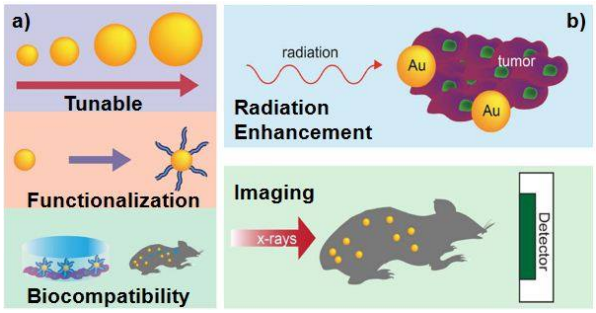

Figure 1: *a)Au Np various shapes and size functionalized with various biomolecules, creating biocojugaties. The suministración can take place in various ways, or by intratumoral injection, intravenously or by means of suitable drugs. b)Np have the ability to enhance radiation therapy of tumors, as well as serve as high-Z imaging contrast agents.*

Target	Absortion Coefficient μ_{Abs}		Stopping Power $\frac{dE}{dx}$	
	50 keV	100 keV	H^+ 60 MeV	e- 1 MeV
H_2O	0,042 cm^{-1}	0,025 cm^{-1}	1,08 MeV/mm	0,19 MeV/mm
CORTICAL BONE	0,43 cm^{-1}	0,083 cm^{-1}	1,875MeV/mm	0,31 MeV/mm

Table I: *Absoption coefficient and stopping power in equivalent tissue and in bone cortical for X-ray of 50 and 100 keV, protons of 60 MeV and elecrons of 1 MeV.*

Fig.1 shows that the Au Np can be easily obtained in different shapes and sizes, and has a surface chemistry properties easily controllable that permits functionalization with various biologically molecules. The Au biological activation help to improve the stability, tumor targeting, and the crossing biophysical barriers. Fig.1 shows Au Np of various shapes and sizes, their functionalization with particular molecules which allow the transfer to the tumor sites via biological processes through the use of drugs or by localized injection into the tumor zone (a). The Np so attached to the tumor have the ability to improve radiotherapy and imaging of localized tumors (b). The high atomic number of gold (Au, Z = 79) permits a high absorption and enhancement of ionizing radiation effects, as well as the X-ray attenuation for high imaging applications [2], as reported in the data shown in Tab.I.

Materials and Methods

The method used for the synthesis of Au nanoparticles is the laser ablation in liquid. It is one of the methods that are called top-down because usually we start from the material in massive form and are reduce the size up to the nanoparticles dispersed in solution. Ablation is the process of removing material from the surface by means of processes of vaporization and ionization. The laser ablation in solution, is a technique that allows obtaining nanoparticles of various metals in different solvents (often water) with relative ease. The experimental set-up is relatively simple; we used a Nd: YAG laser operating at the fundamental frequency (1064nm), with a pulse of 200 mJ and 3 ns duration and with a pulse repetition of 10 Hz, which radiates a gold sample immersed in water. The mass of the sample of gold may be 360 mg placed in 15 ml of water. The concentration of Au nanoparticles, after ablation, is measured by the difference in weight of the sample. In our measurements in aqueous solution is generally used a concentration of about 0.37 mg of Au per ml of water [3, 4]. Simulation programs has been used for the calculation of the coefficients of absorption and of the stopping power of the particles as well as for calculating the range to the uncertainties of the range using the NIST database and the simulation program SRIM [5, 6].

Results

During the laser ablation at the Physics Department of Messina University typically we produce nanoparticles of different size and spheroidal shape.

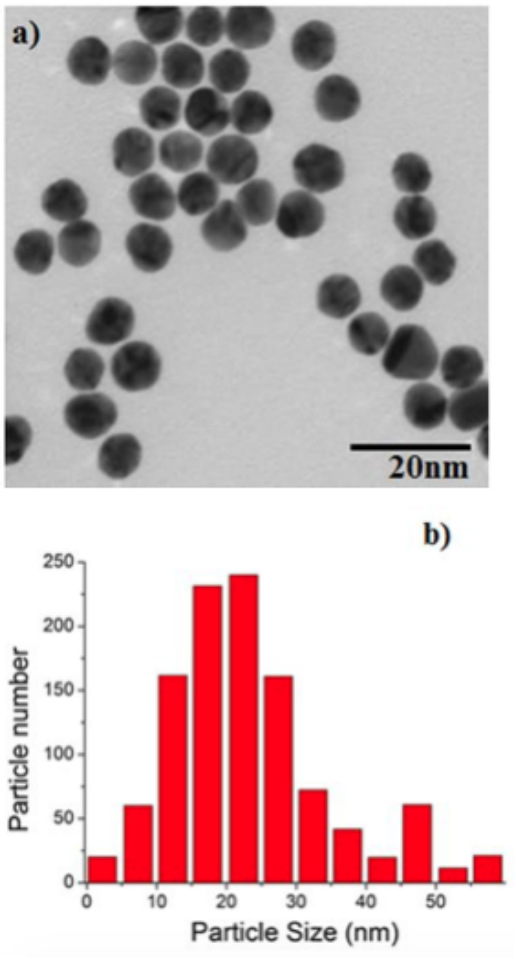

Figure 2: *a) Au Np observed through a transmission electron microscope(TEM). b) size distribution of Np created in laboratory.*

Fig. 2 shows a picture of the transmission electron microscope TEM of Au nanoparticles (a), with a distribution size and average diameter of around 20 nm (b) obtained in our laboratories. The Au nanoparticles absorb and scatter visible light with very hight efficiency. The absorbance is however restricted to a specific band of wavelengths dependent on the size of Np, the form and the nature of surrounding medium. Their strong interaction with light occurs because the conduction electrons on the metal surface undergo collective oscillations when excited by light at specific wavelengths.

This oscillation is known as Surface Plasmon Resonance (SPR), and produces the absorption and scattering of visible light or near UV or IR. The optical properties of spherical Au nanoparticles are strongly dependent on the diameter of the nanoparticles. Smaller nanospheres absorb especially UV light and have peaks near 520 nm with a size of about 20 nm, while the larger spheres show increase of dispersion and have larger peaks at higher wavelengths (known as a red-shifting) as from the literature [7]. Fig. 3 shows the optical density of Au Np in H_2O solution as a function of wavelength and their size (diameter), as reported in the literature [8]. The figure shows that increasing the NP dimension the absoption is shifted toward higher wavelengths. Also NP coalescence phenomenon has a similar behaviour.

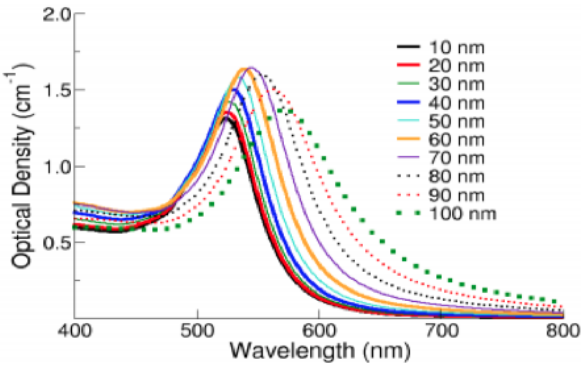

Figure 3: *Optical absorption of Au Np depending on the dimension in the visible range.*

For the purposes of the therapeutic use of directly or indirectly ionazing radiation, it has been proposed to calculate the ratio R between the dose that is released at a given depth and the dose delivered to the surface in various media. Three components were selected as references of biological materials such as water equivalent, adipose tissues and bone compact, evaluating in particular how this ratio varies with the addition of Au nanoparticles. Considering separately the three cases depending on the used radiation: protons, electrons and photons. Only for demonstration purposes it is considered a special geometry, which can then be changed for further analysis with other geometry more or less complex geometry chosen is that of a tumor localized at 3.5 cm depth with 1 cm thickness. In this case, therefore, the first 3 cm surface consist of healthy tissue. Immediately after such a layer is imagined to be tumor of 1 cm thick. In all cases it is considering a certain tumor to about 3 cm deep, and it is supposed that the Au nanoparticles are placed at this depth with a thickness of about 1 cm with the correlation of 0,37 mg/ml. Using NIST and SRIM were evaluated the values of the X-ray absorption coefficients and Stopping Powers of ? radiation in the materials in exam and subsequently employing the Bragg rule to calculate the absorption coefficients or the Stopping Power in the materials with the addition of Au nanoparticles . Fig. 4 represents a simulation study carried out with the data NIST [5] and showing the stopping power of 60 MeV protons released to a tissue constituted by 3 cm water-equivalent plus 1 cm of tumor tissue-equivalent with water and without Au nanoparticles. It is observed that the protons Bragg Peak in the tumor increases by about 17%, compared to water, in the presence of Au nanoparticle (C= 0.37 mg/ml). The nanoparticles thus increase significantly the dose released from the protons to the Bragg peak compared to the case that does not use nanoparticles. In other words this result could also be understood as dose reduction that could be conducted on the tissue at constant radiobiological effect on the tumor. Tab.2 shows the variation of the ratio of dose with and without Au nanoparticles for X-ray 50 and 100 keV, electrons and protons of 1 MeV to 60 MeV.

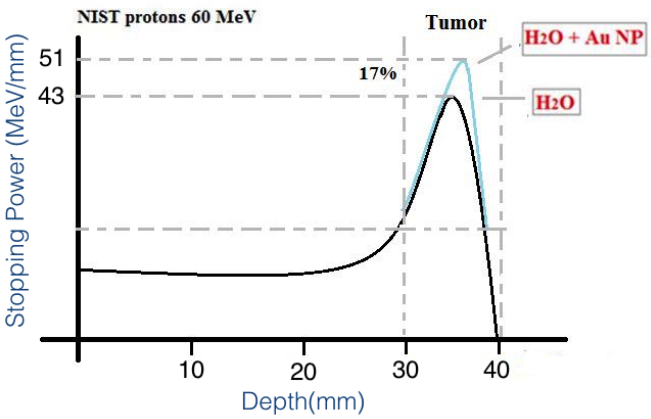

Figure 4: *Variation of Stopping Power as a function of depth for protons evaluated with Nist.*

Target	$R = D_{prof}/D_{sup}$			
	50 keV	100 keV	H^+ 60 MeV	e^- 1 MeV
H_2O	0,9	0,95	40,16	12,11
H_2O+ Au NP (15 wt%)	25,58	26,7	46,88	23,81
CORTICAL BONE	0,27	0,79	44,44	12,38
BONE + Au NP (15 wt%)	0,57	8,2	45,19	18,66

Table II: *Variation of the ratio of dose without and with Au nanoparticles in equivalent tissue and in bone cortical for X-ray of 50 and 100 keV, protons of 60 MeV and elecrons of 1 MeV.*

Discussions and Conclusions

About the use of Au nanoparticles in radiotherapy the best result of studies carried out was obtained for photons, the dose in all tissues examined increases enormously in the layer where it is placed the tumor, thus decreasing the effects on healthy tissues. Even with the electrons experience a strong increase of dose with the addition of nanoparticles. This is mainly due to the fact that the interaction between radiation and matter is strongly dependent on the atomic number Z, as shown by the Bethe-Bloch formula [9] and the cross sections of the processes of photon-matter interaction. In the tissues examined, the Z is very high with the addition of Au nanoparticles and then more energy will be deposited where the nanoparticles are located in the tumor site. These results lead to the conclusion that it is again necessary to optimize the solution containing Au nanoparticles in terms of homogeneity and residence time in suspension. We must do more detailed studies for the delivery of nanoparticles into the tumor site and to distribute them evenly in the tumor site. Moreover, further investigations are being conducted for determining the increase in dose and images contrast in tissues containing Au nanoparticles. Table II shows the variation of the ratio of dose without and with the addition of Au NP in equivalent tissue and in cortical bone for X-rays of 50 keV and 100 keV, for protons of 60 MeV and electrons of 1 MeV.

References

[1] M. A. Garcia "Surface plasmons in metallic nanoparticles:fundamntals and applications" Journal of Physics: Applied Physics 44 (2011) 283001 (20pp).

[2] Jay F. et al. "Gold nanoparticles in radiation research: potential applications for imaging and radiosensitization" Transl Cancer Res 2013;2(4):280-291.

[3] L. Torrisi, M. Cutroneo, G. Ceccio "Effect of metallic nanoparticles in thin foils for laser ion acceleration", PhysicaScripta 90 (2015) 015603 (9pp).

[4] L. Torrisi "Gold ions procuced by 1064 nm pulsed laser irradiation", Nuclear Instruments and Methods in Physics Research B 183 (2001) 271-278.

[5] S. Seltzer Radiation Research 136, 147 (1993).

[6] J. F. Ziegler and J. P. Biersack and M. D. Ziegler (2008). SRIM - The Stopping and Range of Ions in Matter.

[7] Actual Web site 2015: http://www.sigmaaldrich.com/italy.

[8] Actual Web site 2015: http://nanocomposix.eu/collections/gold.

[9] W.R. Leo, Techniques for physics experiments, Lausanne (1987), 17-63.

Simple and rapid synthesis of iron oxide nanoparticles by a high-power picosecond pulsed laser ablation process in water

M. Santoro[1], E. Fazio[1], G. Leonardi[2], G. Neri[2], F. Neri[1]

[1] *Dipartimento di Scienze Matematiche e Informatiche, Scienze Fisiche e Scienze della Terra, viale F. Stagno d'Alcontres 31, Messina, Italy*
[2] *Dipartimento di Ingegneria, Università di Messina, 98166 Messina, Italia*

E-mail: marco.santoro@unime.it

Abstract

Nanostructured iron oxide particle water colloids were prepared by a pulsed laser ablation procedure. Phase-controlled iron oxide nanoparticles were prepared in water. Elemental composition of the Fe_xO_y nanoparticles was determined by X-ray photoelectron spectroscopy (XPS) while the structural and morphological properties were investigated by micro-Raman spectroscopy and Scanning Electron Microscopy (SEM). Pulsed laser ablation procedure adopted reveals a fast and clean technique to obtain, in a one step and in a relatively short time (few minutes), Fe_2O_3 nanostructures with a well defined composition and morphology. Electrical resistance response varying temperature and ethanol concentration was tested collecting the resistance data in the four point mode.

Keywords: iron oxide nanoparticles, pulsed laser ablation, Raman, XPS, SEM, electrical properties.

Introduction

Nowadays, due to the ever increasing standard of living, the sensor technology market is recently expanding and the application of gas sensors has become indispensable in some fields (food industry, medical care and emission controlling). Solid state gas sensors, among which chemi-resistors based on semiconducting metal oxides, are the most extensively applied type, enable in situ and real time measures in various conditions (i.e. high temperature) [1].

Among the metal oxide based sensors, $\alpha - Fe_2O_3$ nanostructures are commonly used as gas sensor materials in contrast to the metastable $\beta - Fe_2O_3$ or Fe_3O_4 ones [2], thanks to their low cost and nontoxicity. Nevertheless, some drawback limits their effective applications. Due to the low oxidation stability of Fe_3O_4, its application is restricted to oxygen and humidity free atmospheres even at elevated temperature as required in the field of metal processing and fermentation processes. Nowadays, ethanol sensors are industrially applied in selective catalytic reduction reactions of automobiles and coal power plants. However, the sensor response towards ethanol is limited by the iron oxide based sensors cross sensitivity towards other reducing analyte gases such as CH_4, NO, H_2 or towards formaldehyde vapors which can affect the immune system of human health and a limited operation temperature range (until $350°C$) [3].

In this contest, the synthesis of iron oxide nanoparticles with a controlled composition and an high specific surface is required in order to optimize the sensor performance and working temperature [4].

Regarding the synthesis procedure to adopt, it emerges that the laser ablation represents a fast and green technique to obtain Fe_2O_3 nanostructures with a well defined composition and morphology [5]. Unlike the chemical approach, no post-preparation purification procedure is necessary adopting the pulsed laser ablation technique. However, the optimal preparation conditions to have Fe_2O_3 nanostructures with defined structural and morphological properties useful to increment gas sensors performance are not well established.

Thus, the overall aim of this work is to explore the possible to use of "in liquid" laser irradiation approaches in order to prepare iron oxide nanoparticles chemically and morphologically stable with a narrow size distribution and, hence, to estimate their electrical resistance response varying temperature and the ethanol concentration.

Experimental section

FeO nanostructured colloidal solutions are synthesized by pulsed laser ablation in liquid (PLAL). By definition, the laser ablation is the ejection of macroscopic amount of materials from the surface of a solid induced by the repetitively interaction of a short ($10^{-13} - 10^{-8}\,s$), intense ($10^6 - 10^{14}\,W/cm^2$) laser pulses with the surface [6]. Briefly, a plasma is generated in water ($5\,ml$) by the impact of a pulsed laser

beam onto a metallic Fe (99.99% of purity) and confined in the surrounding liquid. During the ablation process, the high power laser beam is focused onto the target surface, leading to a plume formation in which both ablated species and small amount of water are vapourized to form a plasma within the liquid. Chemical reactions between the ablated species and the liquid molecules are likely to occur and the high temperature (estimated of the order of thousands of Kelvin degrees) and pressures (in the range of GPa) reached inside the plume allow the iron oxide nanoparticles formation [7]. The incident beam is the second harmonic ($532\,nm$) of a Coherent laser (pulse duration $6-8\,ps$, repetition rate $100\,KHz$). The laser ablation is performed fixing the laser fluence at $0.6\,J/cm^2$ and the ablation time at $2\,min$. These values ensure to observe appreciable spectroscopic signals from the colloids, preventing any possible degradation. X-ray photoelectron spectroscopy (XPS) spectra were acquired using a K-Alpha system of Thermo Scientific, equipped with a monochromatic Al K-Alpha source ($1486.6\,eV$) and operating in constant analyzer energy (CAE) mode with a pass energy of $20\,eV$ for high resolution spectra and a spot size of $400\,mm$. The micro-Raman responses of the materials were investigated after the deposition of some drop of the water colloids on a CaF_2 substrates. Raman spectra were excited by the $638\,nm$ radiation of a $30\,mW$ diode laser, for an integration time of $80\,s$. The backscattered radiation, collected by an Olympus BX 40 microscope optics using a $50X$ objective lens, was analyzed by an XploRA $1800\,cm^{-1}$ monochromator equipped with a Peltier CCD sensor. A fraction of the same colloids was deposited on carbon substrates to carry out Scanning Electron Microscopy (SEM) characterization. SEM images were taken by a scanning electron microscope (Merlin; model ZEISS-Gemini 2) operating at an accelerating voltage of $3\,KV$. When the measure was carried out in transmission mode (STEM), the images were acquired using an accelerating voltage of $30\,KV$ and at a working distance of $4\,mm$. Finally, the study of electrical properties of the sample in terms of electrical resistance for technological applications in the sensoristic field are carried out. Devices for the sensing tests were fabricated by printing films ($1-10\,\mu m$ thick) of the iron oxide nanocolloids on alumina substrates ($6\,mm \times 3\,mm$) with Pt interdigitated electrodes. A Pt heater was located on the backside of the electrodes. Electrical measurements were carried out in the temperature range from RT to $450°C$, under a controlled ethanol gas flux (from $100\,ppm$ up to $500\,ppm$), collecting the resistance data in the four point mode. More details about the sensing tests procedure are reported in Ref. [8] where the CO_2 sensing properties of $ZnO:Ca$ nanopowders are reported.

Results and discussion

The chemical composition of the sample was determined using the Scofield's sensitivity factors supplied with the ThermoAvantage analysis software. XPS analysis show the presence in the sample of C (39%), O(43%), Fe (16%), Na (1%) and Cl (1%).

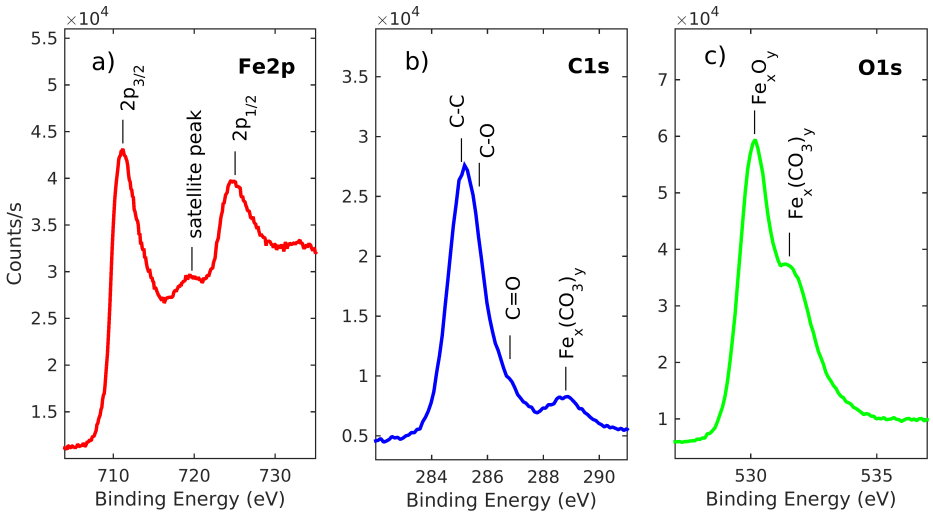

Figure 1: *Fe_{2p}, C_{1s} and O_{1s} lineshapes for the PLAL iron oxide sample.*

Information about the bonding fractions are obtained by the high resolution XPS profiles of the recorded atomic species. Figure 1 shows the C_{1s}, O_{1s} and Fe_{2p} photoemission spectra of the investigated sample. Fe_{2p} lineshape is characterized by three main contributions, ascribed to the $Fe_{2p3/2}$ and $Fe_{2p1/2}$ spin-orbit components, centred at 710.7 and 724.2 eV, respectively and to the satellite peak at about 719 eV [9]. According to these evidences, the hematite $\alpha - Fe_2O_3$ and maghemite $\gamma - Fe_2O_3$ phases coexist in our sample. Furthermore, C_{1s} profiles are characterized by different contributions: a main contribution at 284.5 eV attributed to $C = C/C - C$ in the aromatic ring and other contributions at higher binding energies corresponding to carbon atoms bonded to iron ($Fe_x(CO_3)_y$), centred at about 288.5 eV, and to oxygen atoms in different surface functionalities ($C-O$, $C=O$), centred at 285.2 and 288.9 eV, respectively [10]

In Figure 2 is shown the corresponding Raman spectrum. It is characterized by some contributions centred at about 226.8, 292.5, 400, 486.5 and 600 cm^{-1}, ascribed to the $Fe-O$ vibrational stretching modes in the hematite phase ($\alpha - Fe_2O_3$) [11]

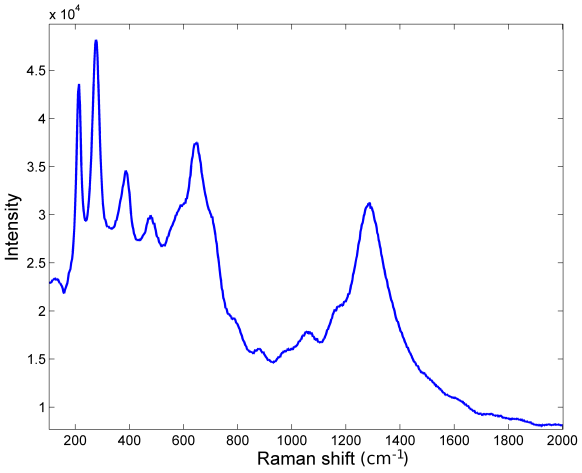

Figure 2: *Raman spectrum of the PLAL synthesized sample.*

In addition, the Raman spectrum of this sample is characterized by a contribution with an intensity comparable to ones ascribed to the Fe_2O_3 phase, centred at about 1350 cm^{-1}. This contribution could be due to the $Fe-C$ or $C-C$ bonds vibrational modes [12]

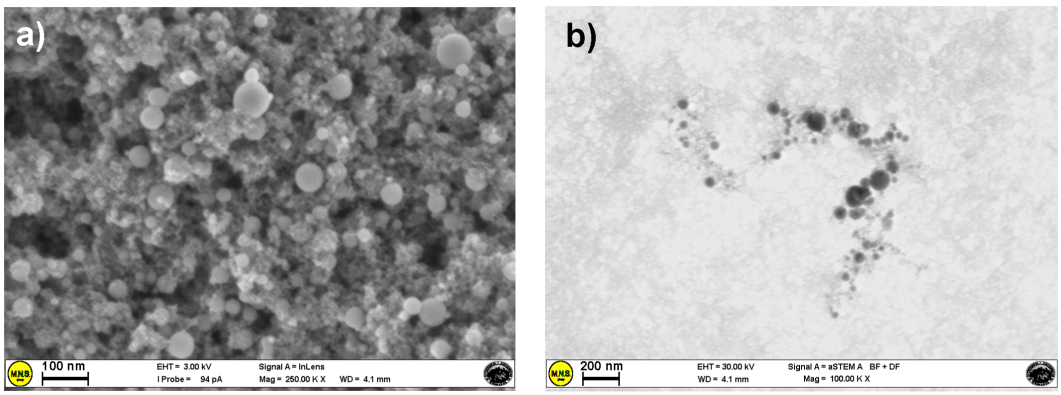

Figure 3: *(a) SEM and (b) STEM images of the PLAL synthesized sample.*

In Figure 3 are shown SEM and STEM images of the sample prepared in water at the laser power of 0.5 W. Scanning electron microscopy images show spherical nanoparticles with dimensions ranging between 20 and 100 nm.

Finally, sensing test were carried out to evaluate the response of Fe_2O_3 nanostructured sensor to ethanol gas. At room temperature, a monotonous reduction of the electrical resistance is observed upon increasing the temperature (see Figure 4).

Moreover, the material is sensible, in a reversible way, to ethanol: a reduction of the resistance values has been collected during the sensor exposure at the gas. Once the sensor is exposed to air, the resistance values return to the initial ones (see Figure 4). Based on the results reported above, it appears plausible that ethanol adsorption on the sensing layer plays a determinant role in the sensing mechanism. How-

ever, these results are only preliminary and a more accurate study of the sensing mechanisms will made in future.

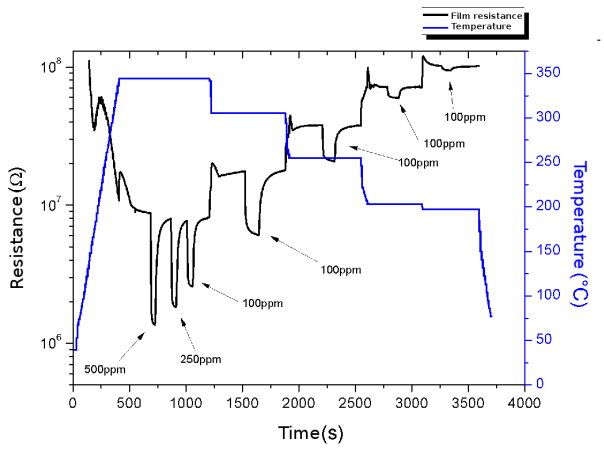

Figure 4: *Electrical resistance response varying temperature and ethanol concentration.*

Conclusions

The procedure of a laser-induced ablation of a iron target in a liquid environment, that is a pure water, is described and discussed. The compositional, structural and morphological properties of the Fe_2O_3 nanoparticles are analyzed. The results show that the high-power pulsed laser ablation technique allows to obtain samples with a controlled composition/phase as well as a tailored particles size distribution in order to make the material suitable for applications in chemical resistant gas sensing fields.

References

[1] C.J. Belle, A. Bonamin, S. Ulrich, J. Santoyo-Salazar, M. Pauly, S. Bègin-Colin, G. Pourroy, Sensor and Actuators B, **160**, 2011, p. 942–950.

[2] N. Duc Cuong, T.T. Hoa, D.Q. Khieu, T. Dai Lam, N. Duc Hoa, N. Van Hieu, Journal of Alloys and Compounds, **523**, 2012, p. 120–126.

[3] P. Das, B. Mondal, K. Mukherjee, RSC Adv., **4**, 2014, p. 31879–31886.

[4] S. Liang, H. Bi, J. Ding, J. Zhu, Q. Han, X. Wang, Ceramics International, **41**, 2015, p. 6978–6984.

[5] S. Dadashi, R. Poursalehi, H. Delavari, Procedia Materials Science, **11**, 2015, p. 722–726.

[6] E. Fazio, A. Cacciola, A.M. Mezzasalma, G. Mondio, F. Neri, R. Saija, Journal of Quantitative Spectroscopy & Radiative Transfer, **124**, 2013, p. 86–93.

[7] P. Liu, W. Cai, H. Zeng, J. Phys. Chem. C, **112** (9), 2008, p. 3261–3266.

[8] R. Dhahri, M. Hjiri, L. El Mir, E. Fazio, F. Neri, F. Barreca, N. Donato, A. Bonavita, S.G. Leonardi, G. Neri, J. Phys. D: Appl. Phys., **48**, 2015, p. 255503–255510.

[9] V. Rebuttini, E. Fazio, S. Santangelo, F. Neri, G. Caputo, C. Martin, T. Brousse, F. Favier, N. Pinna, Chemical Modification of Graphene Oxide-Iron Oxide Nanocomposites In: Chemistry-A European Journal, **21**, 2015, p. 1–11.

[10] S.L. Wu, Z.D. Cui, F. He, Z.Q. Bai, S.L. Zhu, X.J. Yang, Materials Letters, **58**, 2004, p. 1076–1081.

[11] S.H. Shime,T.S. Duffy, Am. Mineral **87**, 2001, p. 318–326.

[12] A. Wang, K. Kuebler, B. Jolliff, L.A. Haskin, J. Raman Spectroscopy, **35**, 2004, 504.